



HAL
open science

Enhancing oxygen reduction reaction of YSZ/La₂NiO_{4+δ} using an ultrathin La₂NiO_{4+δ} interfacial layer

Messaoud Benamira, Armelle Ringuedé, Michel Cassir, David Horwat, Pascal Lenormand, Florence Ansart, Jean-Marc. Bassat, Jean-Paul Viricelle

► **To cite this version:**

Messaoud Benamira, Armelle Ringuedé, Michel Cassir, David Horwat, Pascal Lenormand, et al.. Enhancing oxygen reduction reaction of YSZ/La₂NiO_{4+δ} using an ultrathin La₂NiO_{4+δ} interfacial layer. *Journal of Alloys and Compounds*, 2018, 746, pp.413-420. 10.1016/j.jallcom.2018.02.339 . hal-01744173

HAL Id: hal-01744173

<https://hal.science/hal-01744173>

Submitted on 21 Oct 2019

HAL is a multi-disciplinary open access archive for the deposit and dissemination of scientific research documents, whether they are published or not. The documents may come from teaching and research institutions in France or abroad, or from public or private research centers.

L'archive ouverte pluridisciplinaire **HAL**, est destinée au dépôt et à la diffusion de documents scientifiques de niveau recherche, publiés ou non, émanant des établissements d'enseignement et de recherche français ou étrangers, des laboratoires publics ou privés.





Open Archive Toulouse Archive Ouverte (OATAO)

OATAO is an open access repository that collects the work of Toulouse researchers and makes it freely available over the web where possible

This is an author's version published in: <http://oatao.univ-toulouse.fr/24536>

Official URL: <https://doi.org/10.1016/j.jallcom.2018.02.339>

To cite this version:

Benamira, Messaoud and Ringuède, Armelle and Cassir, Michel and Horwat, David and Lenormand, Pascal  and Ansart, Florence  and Bassat, Jean-Marc and Viricelle, Jean-Paul *Enhancing oxygen reduction reaction of YSZ/La₂NiO_{4+δ} using an ultrathin La₂NiO_{4+δ} interfacial layer.* (2018) *Journal of Alloys and Compounds*, 746. 413-420. ISSN 0925-8388

Any correspondence concerning this service should be sent to the repository administrator: tech-oatao@listes-diff.inp-toulouse.fr

Enhancing oxygen reduction reaction of YSZ/La₂NiO_{4+δ} using an ultrathin La₂NiO_{4+δ} interfacial layer

M. Benamira ^{a, b, *}, A. Ringuedé ^b, M. Cassir ^b, D. Horwat ^c, P. Lenormand ^d, F. Ansart ^d, J.M. Bassat ^e, J.P. Viricelle ^f

^a Laboratory of Interaction Materials and Environment (LIME), University of Mohamed Seddik Ben Yahia, 18000, Jijel, Algeria

^b PSL Research University, Chimie Paristech-CNRS, Institut de Recherche de Chimie de Paris, 11 rue Pierre et Marie Curie, F-75231, Paris Cedex 05, France

^c Institut Jean Lamour, UMR7198, Université de Lorraine, 54011, Nancy, France

^d CIRIMAT/LCMIE/UMR5085, Université Paul Sabatier, bât IIR1, 118, route de Narbonne, 31062, Toulouse Cedex 04, France

^e CNRS, ICMCB, 87 avenue du Dr. A. Schweitzer, F-33608, Pessac, France

^f Ecole Nationale Supérieure des Mines, SPIN-EMSE, CNRS: UMR5307, LGF, 42023, Saint-Etienne, France

ARTICLE INFO

Keywords:

SOFCs

La₂NiO_{4+δ} cathode

Ultrathin film

Sputtering

Dip-coating

ABSTRACT

In this work, La₂NiO_{4+δ} is used as cathode material for Intermediate temperature solid oxide fuel cells (IT SOFC). Scanning electron microscopy, X ray diffraction, and electrochemical impedance spectroscopy are used to investigate the effect of the presence of an ultrathin La₂NiO_{4+δ} layer (80 nm) deposited by dip coating or sputtering at the interface YSZ/La₂NiO_{4+δ}. The thick porous cathode layer of La₂NiO_{4+δ} is deposited by screen printing, and sintered at 1000 °C for 2 h or 1200 °C for 20 min in order to study the effect of sintering temperature on the electrochemical properties. The results show that the electrochemical performances of the cathode are influenced by the deposition technique. The best electrochemical properties are obtained with the use of the nano film interface layer deposited by sputtering. The introduction of ultrathin interface with nano grained between the cathode and electrolyte is a promising technique to reduce polarization resistance associated with oxygen reduction reaction (ORR) on the cathode.

1. Introduction

Solid oxide Fuel cell (SOFC) is a device where the chemical energy is converted to electrical energy. The most important challenge in SOFCs development is the reduction of the working temperature from 800–1000 °C to 500–700 °C which reduces manufacturing costs, owing to use of inexpensive materials, such as stainless steels for interconnects and decreases materials degradation. However, decreasing the temperature leads an increase in the ionic conductivity of the solid electrolyte and in the polarization resistance of the electrodes, in particularly at the cathode side. The ohmic loss is usually decreased by the reduction of the conventional electrolyte thickness, yttria stabilised zirconia (YSZ), or by finding a new material exhibiting a high ionic conductivity [1–5]. For the electrode, the high cathode polarization may be

reduced by improving the microstructure at the interface electrolyte/cathode and/or a development of new cathode materials with high electrochemical activity as the mixed ionic and electronic conductors (MIECs) [6–9].

Recently, the family of compounds A₂MO_{4+δ} with the K₂NiF₄ type structure has attracted more attention as alternative cathode materials for intermediate temperature SOFCs (IT SOFCs) [8,9] due to their high electronic conductivity, thermal expansion coefficients (TECs) close to the solid electrolyte, high electrocatalytic activity, and some oxygen overstoichiometry which enhances the oxygen ionic conduction [10–13]. Among those materials, La₂NiO_{4+δ} has shown a wide range of oxygen overstoichiometry and presents one of the highest oxygen diffusion values [14]. The structure of La₂NiO_{4+δ} is built of alternative rock salt La₂O₂ and perovskite NiO₂ layers, and can contain a significant oxygen excess [14–17]. The ionic transport takes place through diffusion phenomena of interstitial ions in the vacancies in the perovskite layers and the rock salt layer [8,18].

Development of new architecture of SOFCs has been extensively investigated. It is reported that the electrode performance can be

* Corresponding author. Laboratory of Interaction Materials and Environment (LIME), University of Mohamed Seddik Ben Yahia, 18000, Jijel, Algeria.

E-mail address: m_benamira@univ-jijel.dz (M. Benamira).

improved by using an interlayer thin film with fine microstructure at the interface electrolyte/electrode and covered by a thick and porous layer with large grain sizes [19–22]. The fine electrode microstructure close to the electrolyte increases the reaction zone by the enlargement of the triple phase boundary (TPB), the electrochemical active surface area and improved oxygen reduction reaction (ORR) kinetics [15,23].

The present work is focused on the optimisation of thick layer of $\text{La}_2\text{NiO}_{4+\delta}$ obtained by screen printing to analyse their structural and electrochemical performance and compare them in a new configuration with ultrathin layer (80 nm) of $\text{La}_2\text{NiO}_{4+\delta}$ deposited at the interface YSZ/ $\text{La}_2\text{NiO}_{4+\delta}$ by dip coating or sputtering, developed in two laboratories, ^dCIRIMAT and ^eLSGS, respectively. The electrochemical performances of all the samples were realised in the same entity, ^bIRCP.

2. Experimental

2.1. Preparation of electrolyte substrates

The electrolyte substrates are prepared from an YSZ commercial powder containing 8 mol% of Y_2O_3 (TZ8Y from Tosoh Corp, Japan). The powder is pressed into pellets of 19 mm diameter and sintered at 1350 °C for 2 h in air. The density of the samples is up to 95%.

YSZ Pellets are mirror polished with an average roughness of about 10–15 nm and cleaned in ultrasonic baths of acetone and then in ethanol using an ultrasonic bath.

2.2. Preparation of precursor and deposition of $\text{La}_2\text{NiO}_{4+\delta}$ ultrathin film with dip coating or sputtering

The Lanthanum nickelates ultrathin films (80 nm) were sputter deposited on glass slides and YSZ substrates by co sputtering of La and Ni metallic targets in the presence of a reactive argon–oxygen gas mixture. The experimental device is a 40 L sputtering chamber pumped down via an oil diffusion suction system allowing a base vacuum of about 10^{-4} Pa, equipped with two targets separated by 100 mm with a rotating substrate holder positioned parallel to the target surfaces as shown in Ref. [24]. In addition, the target to substrate distance was set to 50 mm for the La target and to 80 mm for the Ni target. The substrate was positioned at 50 mm from the center of the substrate holder. The La targets, 50 mm in diameter, are mounted on unbalanced magnetrons and were powered by Advanced Energy generators. The Ni target was powered using an advanced energy direct current MDX 1.5 K generator and the La target was powered using an advanced energy pulsed DC Pinnacle +5 kW generator. The argon and oxygen flow rates were set to 30 sccm for argon and 10 sccm for oxygen and resulted in a working pressure of 0.5 Pa. The discharge current applied to the La and Ni targets were 1 A and 0.1 A for the La and Ni target, respectively. These conditions allowed obtained a La/Ni ratio of atomic concentrations of 2 as shown in a previous study conducted on the same deposition chamber [24]. Coating thickness is determined by the step method with a Talysurf profilometer.

On the other hand, the sol employed for the ultrathin layer deposited by dip coating corresponding to $\text{La}_2\text{NiO}_{4+\delta}$ phase is prepared by using a polymeric route similar to this outlined by Pechini [25]. Pure metal nitrates, $\text{La}(\text{NO}_3)_3 \cdot 6\text{H}_2\text{O}$ and $\text{Ni}(\text{NO}_3)_2 \cdot 6\text{H}_2\text{O}$ are used as starting salts. They are dissolved in water in stoichiometric amounts [26]. The solution was mixed to an organic solution of hexamethylenetetramine and acetyl acetone with a molar ratio (1:1) in acetic acid. Therefore, a range of molar ratio of complexing agent to nitrate species (called *R*) has been defined. Pure phase is obtained for *R* ratio ranging from 2 to 3. The resulting solution was then stirred and heated in air at 70 °C until

sols. Lanthanum nickelates ultrathin layers are, dip coated on polished mirror Ytria Stabilised Zirconia (YSZ) polycrystalline substrates. The optimal heat treatment to fire the samples is 1000 °C during 2 h in air with a heating rate of 100 °C/h in order to get a well determined oxides structure [26].

2.3. Deposition of $\text{La}_2\text{NiO}_{4+\delta}$ thick cathode by screen printing

The $\text{La}_2\text{NiO}_{4+\delta}$ oxides are prepared using the solid state reaction. A stoichiometric mixture of rare earth oxide (La_2O_3 , Strem, 99.99%) and nickel oxide (NiO, Aldrich, 99.9%) is annealed at 1300 °C and grounded using a milling attritor. After this treatment, the obtained average particle size is around 1 μm.

The screen printing ink is prepared using a $\text{La}_2\text{NiO}_{4+\delta}$ powder mixed with a commercial organic binder (PVB). A solvent is added to obtain adequate ink viscosity (X g of powder with 85% X g of solvent (terpineol) + 4% X g of dispersant (Dolapix) + 14% X g of binder). Ink is deposited on YSZ pellet. The layer is then dried at 120 °C and annealed at 1000 °C for 2 h or 1200 °C for 20 min with a temperature rising rate of 15 °C/min. The whole electrode thickness is about 10–15 μm.

2.4. Microstructural and electrical analysis

Different techniques are used to characterise the YSZ/ $\text{La}_2\text{NiO}_{4+\delta}$ samples. Crystallinity is determined by X ray diffraction (XRD), the microstructure and the thickness of the samples are investigated using scanning electron microscope (SEM) and the electrical properties are analysed by impedance spectroscopy.

The surface morphology and the microstructure of the cross section of the samples are investigated using scanning electron microscope SEM (S440, FEG). The thickness of the deposits is determined from cross sectional SEM micrographs. X ray diffraction analysis is determined using a Co K_α radiation ($\lambda = 1.78897 \text{ \AA}$) with 2θ varying from 25 to 73°. The diffraction pattern is scanned by steps of 0.02° with 2 s counting times.

Electrical measurements are performed by impedance spectroscopy, using a PGSTAT 20 potentiostat, Autolab Ecochemie BV (Amsterdam, Netherlands). Impedance spectroscopy measurements are carried out under ambient atmospheric air as a function of the temperature. A specific two electrode asymmetric configuration is used [27]. With respect to the system linearity, 50 mV ac signal amplitude is applied, without DC polarization. Each impedance measurement is carried out in the 1 MHz–10 MHz frequency range, with 11 points per decade. The temperatures vary from 390 °C to 700 °C. The numbers show in the impedance diagrams indicates the logarithm of the measuring frequency. The impedance data is deconvoluted by the software EQUIVCRT [28].

3. Results and discussion

The X ray diffraction patterns at room temperature for $\text{La}_2\text{NiO}_{4+\delta}$ thick layer deposited by screen printing onto YSZ substrate and annealed at 1000 °C for 2 h or 1200 °C for 20 min are shown in Fig. 1. There is no significant reaction between the $\text{La}_2\text{NiO}_{4+\delta}$ cathode and the electrolyte when the sample is sintered at 1000 °C for 2 h (Fig. 1a). The peaks corresponding to the pure and well crystallized K_2NiO_4 structure (JCPDS, ref. 72 1241) can be observed. However, there is a slight reaction when the $\text{La}_2\text{NiO}_{4+\delta}$ cathode is screen printed onto YSZ and sintered at 1200 °C for 20 min, leading to the formation of impurity phase as shown in (Fig. 1b). According to the literature [29,30], $\text{La}_2\text{NiO}_{4+\delta}$ can be decomposed to produce higher order Ruddlesden Popper ($\text{La}_{n+1}\text{Ni}_n\text{O}_{3n+1}$ where *n* = 2 or 3) and La_2O_3 at higher temperature ($\geq 1150 \text{ °C}$). Gauquelin et al. confirm the presence of $\text{La}_3\text{Ni}_2\text{O}_7$

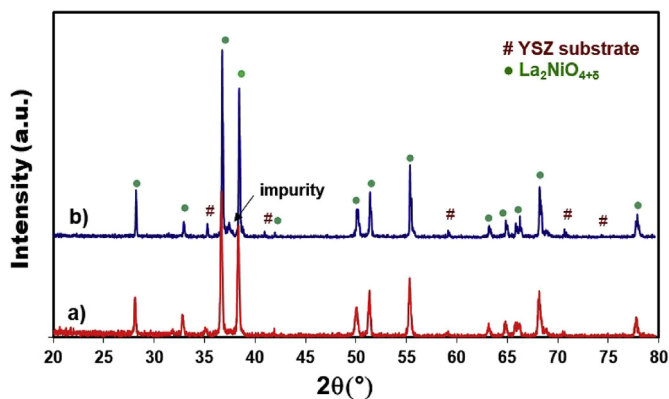


Fig. 1. X-ray diffraction pattern of $\text{La}_2\text{NiO}_{4+\delta}$ cathode deposited by screen-printing and annealed at a) $1000\text{ }^\circ\text{C}/2\text{ h}$ and b) $1200\text{ }^\circ\text{C}/20\text{ min}$.

and $\text{La}_4\text{Ni}_3\text{O}_{10}$ using transmission electron microscopy (TEM) after a long term decomposition experiment of $\text{La}_2\text{NiO}_{4+\delta}$ at $1000\text{ }^\circ\text{C}$ in flowing air for two weeks [31]. This result is also partly confirmed by the theoretical study using density functional theory (DFT) [29]. It should be noted that the formation of $\text{La}_{n+1}\text{Ni}_n\text{O}_{3n+1}$ ($n = 2$ and 3) phases present a beneficial effect with high electrical transport properties (high electronic conductivity) [32–34]. No decomposition of $\text{La}_2\text{NiO}_{4+\delta}$ or chemical reaction with YSZ were found at $1000\text{ }^\circ\text{C}$. Nevertheless, reactivity or decomposition were observed at $1200\text{ }^\circ\text{C}$ according to DRX (Fig. 1).

The sintering temperature dramatically affects the microstructure of the electrode. Fig. 2 shows the SEM micrographs for $\text{La}_2\text{NiO}_{4+\delta}$ films sintered at $1000\text{ }^\circ\text{C}$ and $1200\text{ }^\circ\text{C}$. It can be seen that fine and smaller particles can be obtained when the sintered temperature decreased ($1000\text{ }^\circ\text{C}$). The sample sintered at $1200\text{ }^\circ\text{C}$

possesses low porosity and inhomogeneous pore size distribution. The comparison of the figures of the two samples illustrates the coarsening of the $\text{La}_2\text{NiO}_{4+\delta}$ microstructure that occurs with the annealing. Larger particle sizes decrease not only the porosity but also the TPB and limits the gas transport in the gas phase to the electrode, leading to the decrease in electrochemical reaction area.

The cross section SEM micrographs of the two samples are shown in Fig. 3. It can be seen that the $\text{La}_2\text{NiO}_{4+\delta}$ cathode and the YSZ electrolyte attached well. Indeed, it is clearly shown the high densification of the electrolyte and the porosity of the cathode film. The thickness of the cathode for the two samples is around $13\text{--}15\text{ }\mu\text{m}$ (Fig. 3a, c). Homogeneous distribution of particles and pores is shown throughout the whole electrode thickness, particularly in the sample sintered at $1000\text{ }^\circ\text{C}$ (Fig. 3a). The difference in the particles sizes and porosity between the two samples is well observed. Large and coarse particles are obtained after $1200\text{ }^\circ\text{C}$ anneal of 20 min. The interface between the $\text{La}_2\text{NiO}_{4+\delta}$ cathode and the YSZ electrolyte are shown in more detail in Fig. 3b, d. It can be observed the presence of a new phase with small particles at the interface YSZ/ $\text{La}_2\text{NiO}_{4+\delta}$ for the sample sintered at $1200\text{ }^\circ\text{C}$ (Fig. 3d), which confirms the impurity phase observed in the X ray diffraction (Fig. 1b). However, no significant reaction between the $\text{La}_2\text{NiO}_{4+\delta}$ cathode and the electrolyte is observed when the sample is sintered at $1000\text{ }^\circ\text{C}$ (Fig. 3b).

Fig. 4 shows the Arrhenius plots of the polarization resistance of the two samples with $\text{La}_2\text{NiO}_{4+\delta}$ thick screen printed layer and annealed at $1000\text{ }^\circ\text{C}$ and $1200\text{ }^\circ\text{C}$. For the thick cathode layer deposited onto YSZ, the lowest polarization resistances are found for the $\text{La}_2\text{NiO}_{4+\delta}$ sintered at $1000\text{ }^\circ\text{C}$. The decrease of performance of sample sintered at $1200\text{ }^\circ\text{C}$ can be attributed to the degradation of the interface YSZ/ $\text{La}_2\text{NiO}_{4+\delta}$ with the formation of ion blocking phase at the interface as it can be seen in the X ray diffraction and SEM micrograph of Figs. 1 and 3. In order to confirm this result, two samples of YSZ/ $\text{La}_2\text{NiO}_{4+\delta}$ with an ultrathin interfacial layer

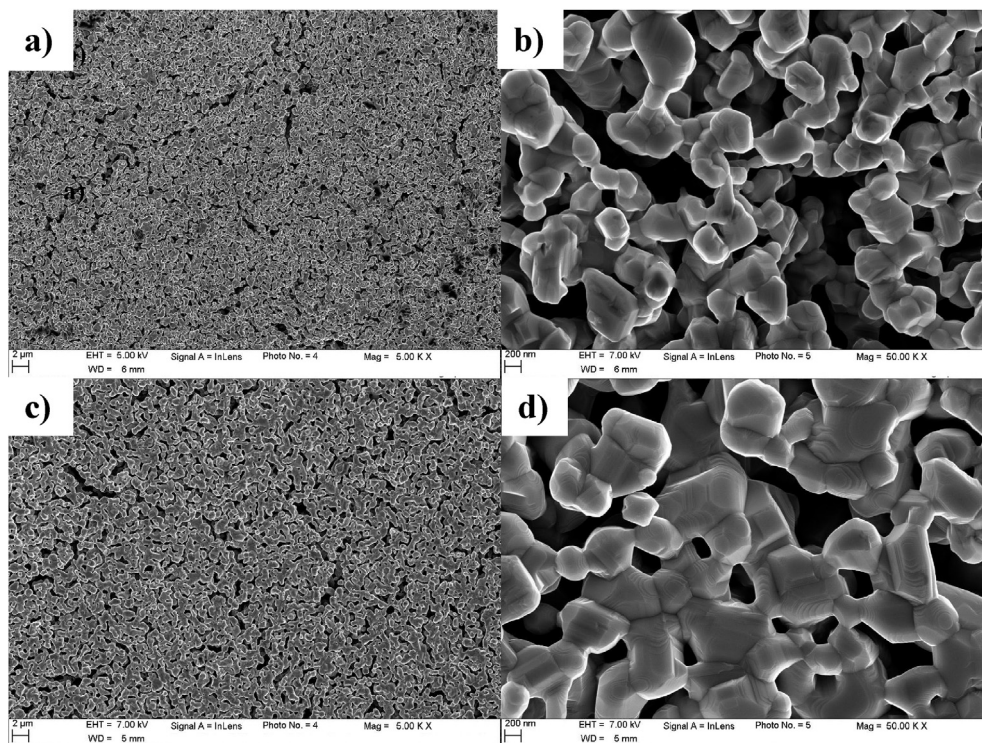


Fig. 2. SEM micrographs of surface morphology of $\text{La}_2\text{NiO}_{4+\delta}$ thick layer deposited by screen-printing onto YSZ electrolyte and annealed at a, b) $1000\text{ }^\circ\text{C}/2\text{ h}$ and c, d) $1200\text{ }^\circ\text{C}/20\text{ min}$.

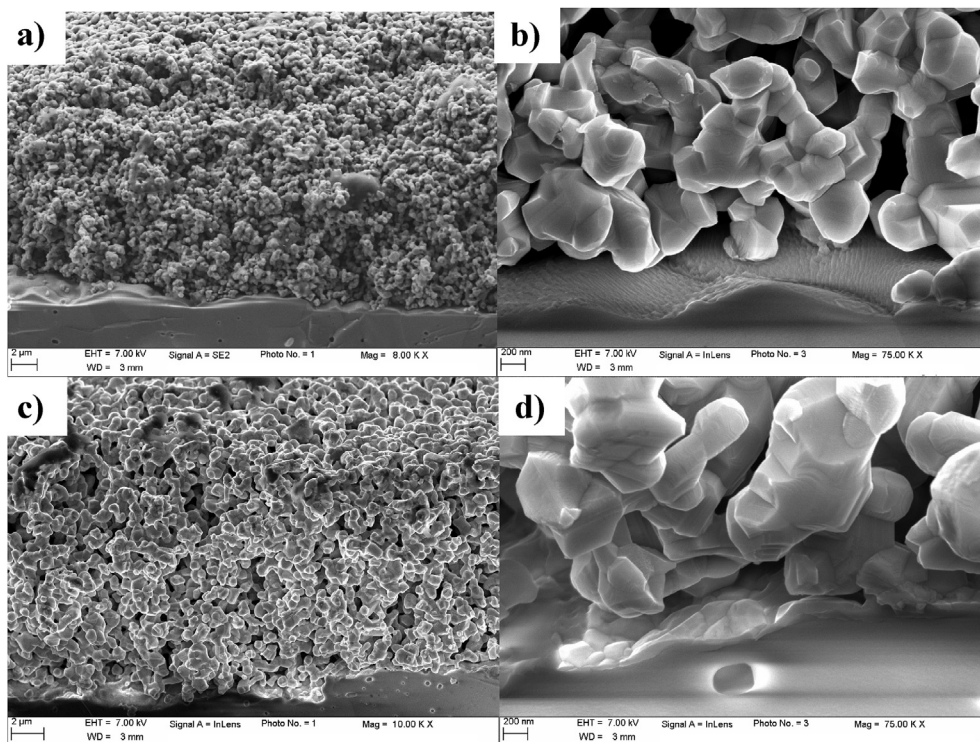


Fig. 3. SEM micrographs of cross-section of $\text{La}_2\text{NiO}_{4+\delta}$ thick layer deposited by screen-printing onto YSZ electrolyte and annealed at a, b) $1000\text{ }^\circ\text{C}/2\text{ h}$ and c, d) $1200\text{ }^\circ\text{C}/20\text{ min}$.

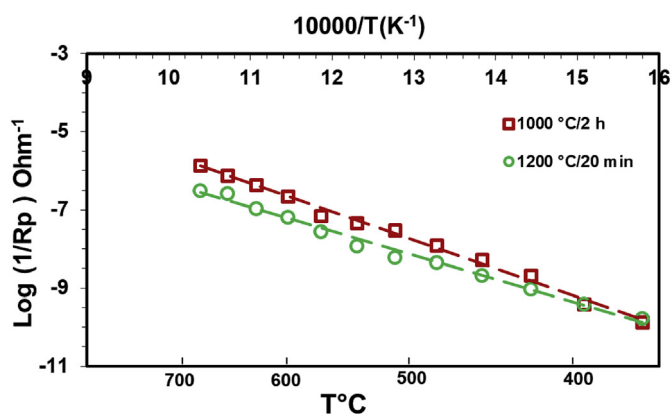


Fig. 4. Arrhenius plots of the polarization resistance for $\text{La}_2\text{NiO}_{4+\delta}$ cathode deposited by screen-printing onto YSZ electrolyte and annealed at: \square) $1000\text{ }^\circ\text{C}/2\text{ h}$, \circ) $1200\text{ }^\circ\text{C}/20\text{ min}$.

deposited by dip coating are prepared and annealed at $1000\text{ }^\circ\text{C}$ for 2 h and $1200\text{ }^\circ\text{C}$ for 20 min. Fig. 5 shows SEM micrographs of the surface morphology and the cross section of the fractured surface of the ultrathin films deposited at the interface $\text{YSZ}/\text{La}_2\text{NiO}_{4+\delta}$ by dip coating onto YSZ substrate. After annealing of the ultrathin films at $1000\text{ }^\circ\text{C}$ for 2 h, the SEM micrographs show that the fired film exhibits small pores as well as small solid phase islands. The microstructure presents a homogeneous distribution of the islands sizes and is very fine. The particle sizes in the ultrathin layer are clearly much smaller than those deposited by screen printing, and the surface appears denser. The X ray diffraction (XRD) patterns at room temperature for $\text{La}_2\text{NiO}_{4+\delta}$ ultrathin layer deposited by dip coating or double layer prepared with ultrathin layer deposited by dip coating and recovered by a thick layer and annealed at $1000\text{ }^\circ\text{C}$ for 2 h and $1200\text{ }^\circ\text{C}$ for 20 min are shown in Fig. 6.

The X ray diffraction analysis reveals that the cathode has a pure and well crystallized K_2NiO_4 structure. The peaks corresponding to the YSZ substrate can be observed. For the YSZ/LSM (dip coating) sample (Fig. 6a), the intensity of the lines corresponding to the $\text{La}_2\text{NiO}_{4+\delta}$ phase is very low compared to the YSZ substrate, which is due to the $\text{La}_2\text{NiO}_{4+\delta}$ ultra thin layer (80 nm) deposited by dip coating. The cathode peaks become well defined when a thick $\text{La}_2\text{NiO}_{4+\delta}$ layer is deposited as it can be seen in the two other samples (Fig. 6b, c). The typical impedance spectra obtained at $600\text{ }^\circ\text{C}$ by impedance spectroscopy of the two samples with interfacial layer of $\text{La}_2\text{NiO}_{4+\delta}$ and annealed at $1000\text{ }^\circ\text{C}$ and $1200\text{ }^\circ\text{C}$ are presented in Fig. 7 a. In general, the spectra measured presents two contributions. The first contribution, in the high frequency range, is smaller (up to 100 KHz), whereas, the second contribution, attributed to the electrode responses, at medium and low frequencies are predominant and well defined in the frequency range used. The impedance diagrams of Fig. 7 a show that the two samples have the same responses at high frequency (HF) which is attributed to grain and grain boundary resistances of YSZ electrolyte [27]. The two other arcs are assigned to the phenomena occurring at the electrode and electrode/electrolyte interface. This indicates that the O_2 reduction on the $\text{La}_2\text{NiO}_{4+\delta}$ cathode is controlled by at least two different processes. The associated equivalent circuit used to fit the experimental data is shown in Fig. 7 b, in which each arc is adjusted to R CPE elements in parallel. The appearance of the arcs in the impedance diagrams are related to the rate determining steps in the oxygen reduction on the $\text{La}_2\text{NiO}_{4+\delta}$ electrode. The medium frequency contribution is assigned to oxygen ion transfer across the electrode/electrolyte interface and charge transfer process, and the low frequency contribution is related to molecular oxygen dissociation, oxygen diffusion through the electrode layer and adsorption phenomena on the porous $\text{La}_2\text{NiO}_{4+\delta}$ surface [35–38].

The low electrode polarization resistance is obtained when the sample is sintered at $1000\text{ }^\circ\text{C}$ for 2 h as it can be seen in Fig. 8. This

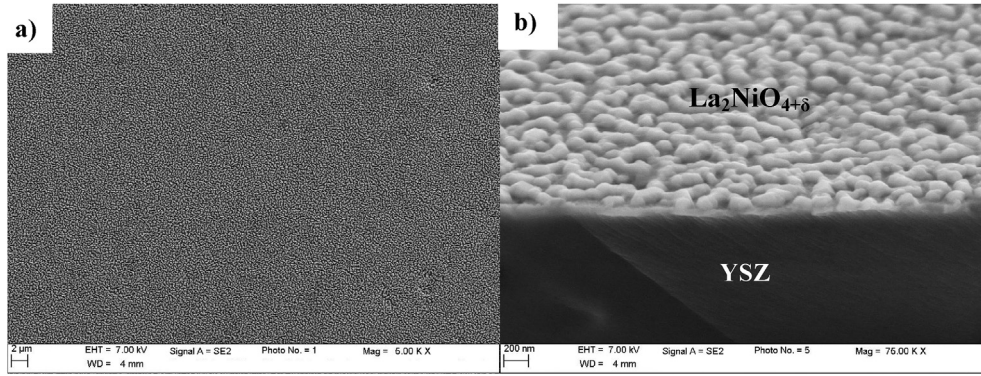


Fig. 5. SEM micrographs of $\text{La}_2\text{NiO}_{4+\delta}$ thin layer deposited by dip-coating onto YSZ electrolyte and annealed at $1000\text{ }^\circ\text{C}/2\text{ h}$, a) surface morphology and b) cross-section.

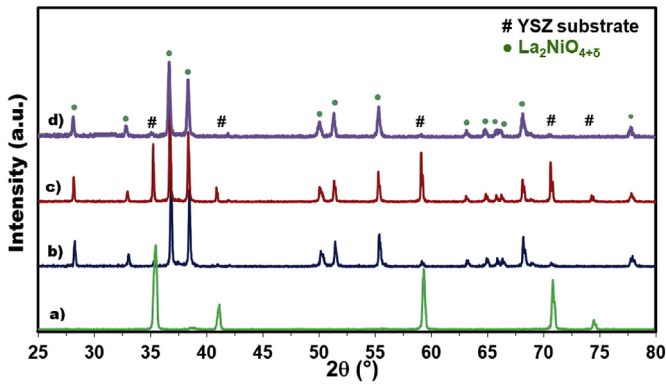


Fig. 6. X-ray diffraction patterns of a) $\text{YSZ}/\text{La}_2\text{NiO}_{4+\delta}$ (dip-coating), $\text{YSZ}/\text{La}_2\text{NiO}_{4+\delta}$ (dip-coating)/ $\text{La}_2\text{NiO}_{4+\delta}$ (screen-printing) annealed at b) $1000\text{ }^\circ\text{C}/2\text{ h}$ and c) $1200\text{ }^\circ\text{C}/20\text{ min}$, d) $\text{YSZ}/\text{La}_2\text{NiO}_{4+\delta}$ (sputtering)/ $\text{La}_2\text{NiO}_{4+\delta}$ (screen-printing).

result can be explained by the relationship between the sintering process of the $\text{La}_2\text{NiO}_{4+\delta}$ and the grains growth with their subsequent coalescence. Fig. 9 illustrates the difference between the effects of 1000 and $1200\text{ }^\circ\text{C}$ temperature sintering on sample microstructure. The SEM micrographs show microstructural changes that can explain the observed result. The thick cathode layers sintered at $1000\text{ }^\circ\text{C}$ for 2 h presents a porous and homogeneous structure, the particles are well connected and the smaller particles coalesced to form larger aggregates (Fig. 9a). The cathode particle sizes are around $0.2\text{--}0.3\text{ }\mu\text{m}$. The particle sizes are less homogeneous; it can be seen small grains size less than $0.1\text{ }\mu\text{m}$ attached to larger grains ($0.4\text{ }\mu\text{m}$). The porosity distribution of the cathode in Fig. 9 b appears less homogeneous than that in Fig. 9 a and the porosity is smaller, due to $200\text{ }^\circ\text{C}$ higher sintering temperature. As a result, the good electrochemical performance of the cathode sintered at $1000\text{ }^\circ\text{C}$ can be attributed to this difference in the microstructure. This temperature is used to sinter the sample

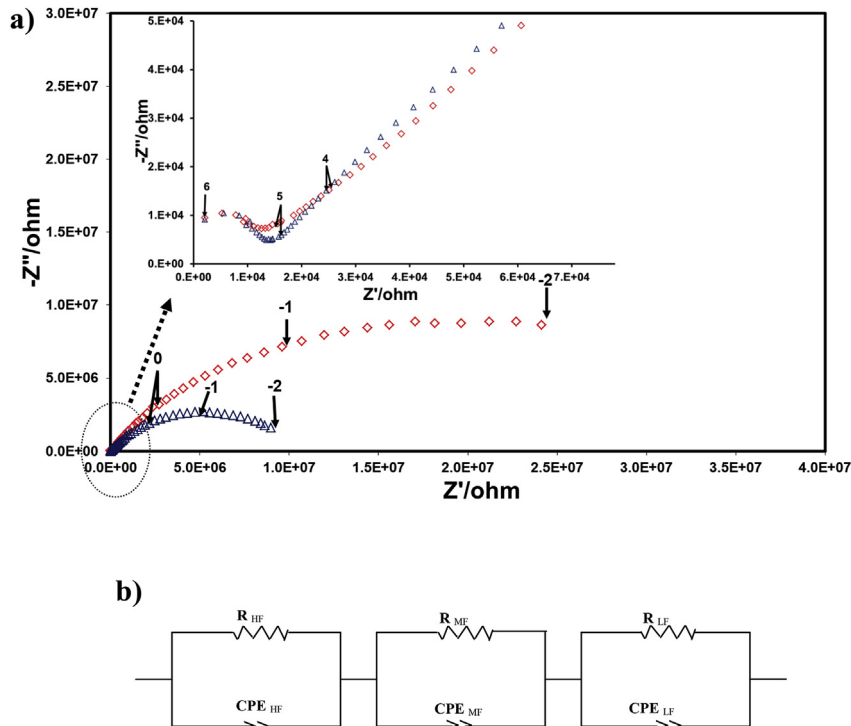


Fig. 7. a) Impedance diagrams measured at $600\text{ }^\circ\text{C}$ under air, 50 mV for $\text{YSZ}/\text{La}_2\text{NiO}_{4+\delta}$ (dip-coating)/ $\text{La}_2\text{NiO}_{4+\delta}$ (screen-printing) samples annealed at Δ) $1000\text{ }^\circ\text{C}/2\text{ h}$ and \diamond) $1200\text{ }^\circ\text{C}/20\text{ min}$ b) Equivalent circuit used for fitting the experimental data.

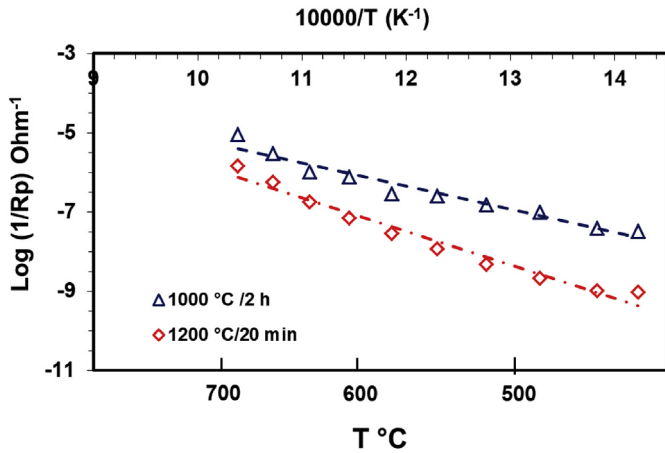


Fig. 8. Arrhenius plots of the polarization resistance for YSZ/La₂NiO_{4+δ}(dip-coating)/La₂NiO_{4+δ} (screen-printing) samples annealed at Δ) 1000 °C/2 h and ◇) 1200 °C/20 min.

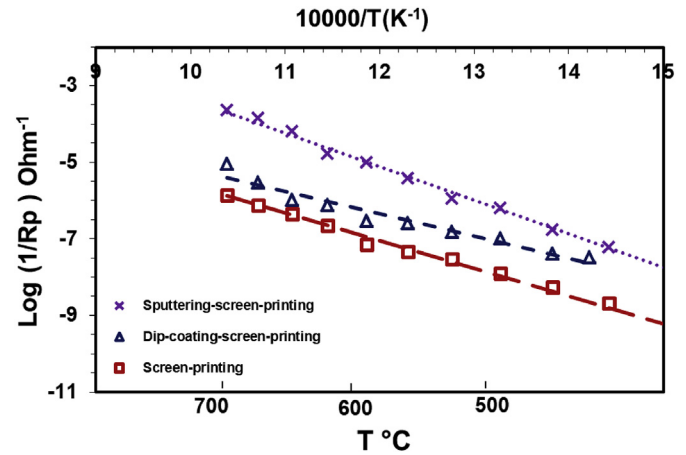


Fig. 10. Arrhenius plots of the polarization resistance of: x) YSZ/La₂NiO_{4+δ}(sputtering)/La₂NiO_{4+δ} (screen-printing) Δ) YSZ/La₂NiO_{4+δ}(dip-coating)/La₂NiO_{4+δ}(screen-printing) and □) YSZ/La₂NiO_{4+δ}(screen-printing) samples annealed at 1000 °C/2 h.

with the La₂NiO_{4+δ} ultrathin interlayer deposited by sputtering. The X ray diffraction of the sample with sputtered ultrathin layer presented in Fig. 6d confirm the presence of a pure and well crystallized K₂NiO₄ structure.

Fig. 10 shows clearly that the polarization resistance (Rp) of the sample with an ultrathin interlayer deposited by sputtering is smaller than that observed of the sample with an interlayer deposited by dip coating and sintered at the same temperature, 1000 °C/2 h. The Rp of cathode decreases by around two orders of magnitude. The significant improvement achieved with a thin La₂NiO_{4+δ} compact layer between the dense electrolyte and porous electrode is a result of contact at the interface YSZ/La₂NiO_{4+δ} enhancing the oxygen ion transfer to the electrolyte. In the temperature range studied here, it is clear that the addition of the compact ultrathin interlayer deposited by dip coating or sputtering reduces the resistances assigned to the electrode processes compared to the electrode/electrolyte without interfacial layer (Fig. 10). The calculated ASR of the best sample with the dense sputtered ultrathin layer at 700 °C is given in Table 1 and compared to those values obtained by other authors with symmetrical cell configurations. The lowest ASR is observed with the presence of a compact layer at the interface electrolyte/cathode. This value is approximately 2 times less than the ASR reported by Zhao et al. [39].

The best performances of sample with interlayer deposited by sputtering can be attributed to the microstructure. Fig. 11 shows the

SEM micrographs of the surface of La₂NiO_{4+δ} cathode deposited onto the ultrathin sputtered layer and the cross section of the fractured surface of the two samples with ultrathin film layers deposited by sputtering or dip coating between the YSZ substrate and the La₂NiO_{4+δ} thick film. The thick cathode layers deposited onto ultrathin sputtered layer (Fig. 11a, b) presents a porous and homogenous structure, the particles are well connected. The cathode particle sizes are around 0.1–0.3 μm. A slight decrease of the particle sizes is obtained in comparison to that observed with cathode deposited onto dip coating ultrathin layer (Fig. 7a). The thickness of the La₂NiO_{4+δ} thin film is about 55–75 nm for the two samples (Fig. 11c, d). It can be observed that the thin layers of La₂NiO_{4+δ} cathode are well bonded to the electrolyte and there is clear difference between the thin La₂NiO_{4+δ} cathode interlayer and the external thick La₂NiO_{4+δ} cathode layer deposited by screen printing. The microstructures of the thin layers appear dense and

Table 1

Summary of ASR of La₂NiO₄ electrode determined by Electrochemical Impedance Spectroscopy at 700 °C.

Reference	Cell configuration	Cathode ASR at 700 °C (Ω. cm ²)
This work	La ₂ NiO ₄ on YSZ	2.1
Zhao et al. [39]	La ₂ NiO ₄ on YSZ	4
Escudero et al. [37]	La ₂ NiO ₄ on YSZ	13.18
Hernández et al. [30]	La ₂ NiO ₄ on YSZ	17.7
Sayers et al. [38]	La ₂ NiO ₄ on CGO	7.4

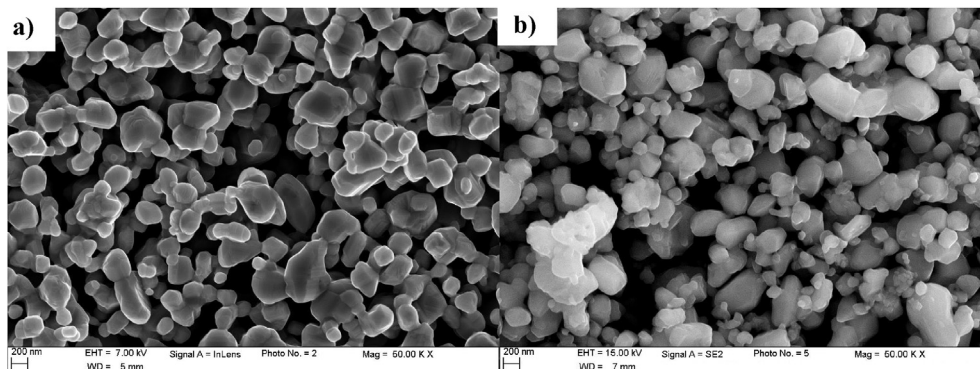


Fig. 9. SEM micrographs of surface morphology of YSZ/La₂NiO_{4+δ}(dip-coating)/La₂NiO_{4+δ} (screen-printing) samples annealed at a) 1000 °C/2 h and b) 1200 °C/20 min.

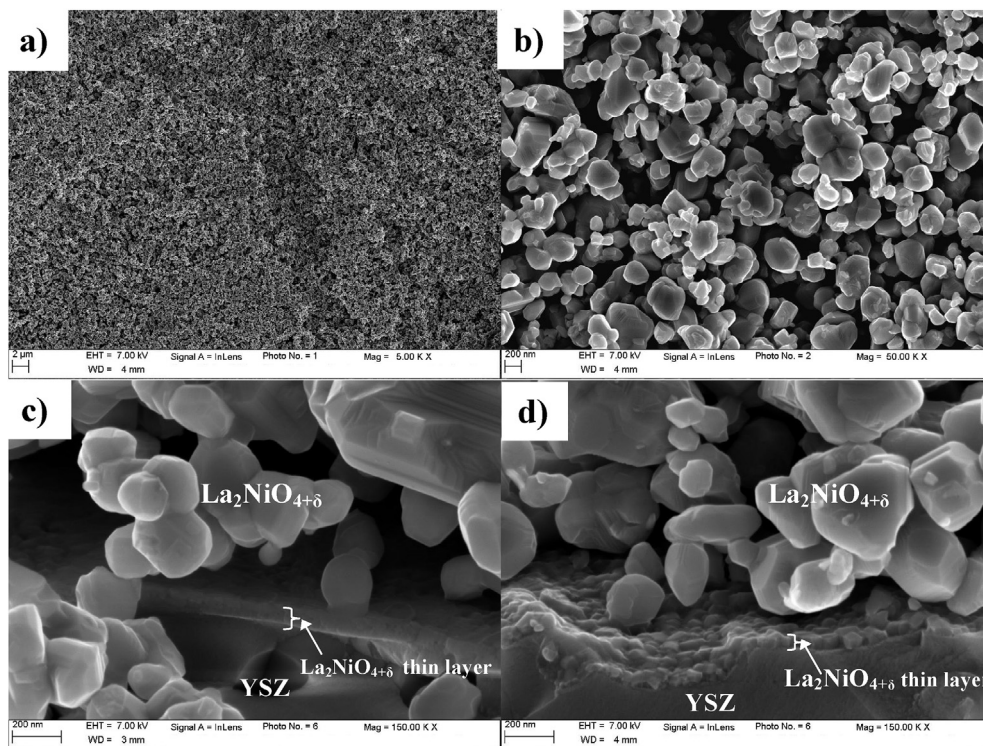


Fig. 11. a, b) SEM micrographs of surface morphology of $\text{La}_2\text{NiO}_{4+\delta}$ cathode deposited by screen-printing onto thin sputtered layer, c) cross-section micrograph of YSZ/ $\text{La}_2\text{NiO}_{4+\delta}$ (sputtering)/ $\text{La}_2\text{NiO}_{4+\delta}$ (screen-printing) sample and d) cross-section micrograph of YSZ/ $\text{La}_2\text{NiO}_{4+\delta}$ (dip-coating)/ $\text{La}_2\text{NiO}_{4+\delta}$ (screen-printing) sample.

lack of porosity. The ultrathin layers are composed of small particles with a good adherence to the YSZ substrates. Furthermore, the particle sizes and the porosity of the ultrathin film at the interface in Fig. 11 c are smaller than those of Fig. 11 d.

It is well known that fine porosity and fine electrode microstructure are desirable for the interface between the electrolyte and cathode to facilitate the charge transfer reaction. The dense cathode film can decrease the triple phase boundary at the interface, limit gas access and charge transfer reaction leading to Rp increase. This phenomenon is observed in Fig. 11 c and can explain the less electrochemical performance compared to the sample with the sputtered ultrathin film. The fine electrode microstructure close to the electrolyte, in this case the ultrathin layer deposited by sputtering, would significantly increase the cathode performance.

4. Conclusion

This work is focused on a study of the influence of the use of an ultrathin layer of $\text{La}_2\text{NiO}_{4+\delta}$ at the interface electrolyte/cathode for SOFC operates at intermediate temperature. SEM micrographs show clearly that the annealing temperature has substantial modifications at the porous $\text{La}_2\text{NiO}_{4+\delta}$ cathode and the interface YSZ/ $\text{La}_2\text{NiO}_{4+\delta}$. The porous electrode sintered at $1200^\circ\text{C}/20$ min degrades faster than the sintered at $1000^\circ\text{C}/2$ h due to the morphological effects of grain growth and their coalescence, interdiffusion across the electrolyte/cathode interface with formation of new ion blocking phases at the interface. Electrochemical impedance spectroscopy demonstrates that the presence of ultra thin sputtered $\text{La}_2\text{NiO}_{4+\delta}$ interlayer with fine microstructure and porosity at the interface between yttria stabilised zirconia electrolyte and thick layer deposited by screen printing improves the electrochemical performance.

Acknowledgments

This work was financed within the frame of the French CNRS (National Research Center for Scientific Research) programs (ACI MICROSOFC).

References

- [1] K. Venkataramana, C. Madhuri, Y.S. Reddy, G. Bhikshamaiah, C.V. Reddy, Structural, electrical and thermal expansion studies of tri-doped ceria electrolyte materials for IT-SOFCs, *J. Alloys. Compd.* 719 (2017) 97–107.
- [2] I. Khan, M.I. Asghar, P.D. Lund, S. Basu, I. Khan, M.I. Asghar, P.D. Lund, S. Basu, High conductive $(\text{LiNaK})_2\text{CO}_3\text{Ce}_0.85\text{Sm}_0.15\text{O}_2$ electrolyte compositions for IT-SOFC applications, *Int. J. Hydrogen Energy* 42 (2017) 20904–20909.
- [3] M. Benamira, A. Ringuedé, L. Hildebrandt, C. Lagergren, R.N. Vannier, M. Cassir, Gadolinia-doped ceria mixed with alkali carbonates for SOFC applications: II an electrochemical insight, *Int. J. Hydrogen Energy* 37 (24) (2012) 19371–19379.
- [4] M. Benamira, A. Ringuedé, V. Albin, R.N. Vannier, L. Hildebrandt, C. Lagergren, M. Cassir, Gadolinia-doped ceria mixed with alkali carbonates for solid oxide fuel cell applications: I. A thermal, structural and morphological insight, *J. Power Sources* 196 (13) (2011) 5546–5554.
- [5] N. Preux, A. Rolle, C. Merlin, M. Benamira, M. Malys, C. Estournes, A. Rubbens, R.-N. Vannier, La_3TaO_7 derivatives with Weberite structure type: possible electrolytes for solid oxide fuel cells and high temperature electrolyzers, *Compt. Rendus Chem.* 13 (2010) 1351–1358.
- [6] S.J. Skinner, J.A. Kilner, Oxygen diffusion and surface exchange in $\text{La}_{2-x}\text{Sr}_x\text{NiO}_{4+\delta}$, *Solid State Ionics* 135 (1) (2000) 709–712.
- [7] C. Lalanne, F. Mauvy, E. Siebert, M.L. Fontaine, J.M. Bassat, F. Ansart, P. Stevens, J.C. Grenier, Intermediate temperature SOFC single cell test using $\text{Nd}_{1.95}\text{NiO}_{4+\delta}$ as cathode, *J. Eur. Ceram. Soc.* 27 (2007) 4195–4198.
- [8] G. Amow, S.J. Skinner, Recent developments in Ruddlesden Popper nickelate systems for solid oxide fuel cell cathodes, *J. Solid State Electrochem.* 10 (2006) 538–546.
- [9] F. Mauvy, C. Lalanne, J.-M. Bassat, J.-C. Grenier, H. Zhao, L. Huo, Ph Stevens, Electrode properties of $\text{Ln}_2\text{NiO}_{4+\delta}$ ($\text{Ln} = \text{La}, \text{Nd}, \text{Pr}$) AC impedance and DC polarization studies, *J. Electrochem. Soc.* 153 (2006) A1547–A1553.
- [10] V.V. Kharton, A.P. Viskup, A.V. Kovalevsky, E.N. Naumovich, F.M.B. Marques, Ionic transport in oxygen-hyperstoichiometric phases with K_2NiF_4 -type structure, *Solid State Ionics* 143 (2001) 337–353.
- [11] J.A. Kilner, C.K.M. Shaw, Mass transport in $\text{La}_2\text{Ni}_{1-x}\text{Co}_x\text{O}_{4+\delta}$ oxides with the K_2NiF_4 structure, *Solid State Ionics* 154–155 (2002) 523–527.

- [12] F. Mauvy, J.M. Bassat, E. Boehm, P. Dordor, J.-P. Loup, F. Mauvy, J.M. Bassat, E. Boehm, P. Dordor, J.P. Loup, Measurement of chemical and tracer diffusion coefficients of oxygen in La₂Cu_{0.5}Ni_{0.5}O_{4+δ}, *Solid State Ionics* 158 (2003) 395–407.
- [13] F. Mauvy, J.-M. Bassat, E. Boehm, J.-P. Manaud, P. Dordor, J.-C. Grenier, Oxygen electrode reaction on Nd₂NiO_{4+δ} cathode materials: impedance spectroscopy study, *Solid State Ionics* 158 (2003) 17–28.
- [14] E. Boehm, J.-M. Bassat, P. Dordor, F. Mauvy, J.-C. Grenier, P. Stevens, Oxygen diffusion and transport properties in non-stoichiometric Ln₂-xNiO_{4+δ} oxides, *Solid State Ionics* 176 (2005) 2717–2725.
- [15] D. Herbstritt, A. Weber, E. Ivers-Tiffée, Modelling and DC-polarisation of a three dimensional electrode/electrolyte interface, *J. Eur. Ceram. Soc.* 21 (2001) 1813–1816.
- [16] M. Al Daroukh, V.V. Vashook, H. Ullmann, F. Tietz, I. Arual Raj, Oxides of the AMO₃ and A₂MO₄-type: structural stability, electrical conductivity and thermal expansion, *Solid State Ionics* 158 (2003) 141–150.
- [17] A. Demourgues, A. Wattiaux, J.C. Grenier, M. Pouchard, J.L. Soubeyroux, J.M. Dance, P. Hagenmuller, A. Demourgues, A. Wattiaux, J.C. Grenier, M. Pouchard, J.L. Soubeyroux, J.M. Dance, P. Hagenmuller, Electrochemical preparation and structural characterization of La₂NiO_{4+δ} phases (0 ≤ δ ≤ 0.25), *J. Solid State Chem.* 105 (1993) 458–468.
- [18] A.A. Yaremchenko, V.V. Kharton, M.V. Patrakeev, J.R. Frade, p-Type electronic conductivity, oxygen permeability and stability of La₂Ni_{0.9}Co_{0.1}O_{4+δ}, *J. Mater. Chem.* 13 (2003) 1136–1144.
- [19] S. Molin, P.Z. Jasinski, Improved performance of LaNi_{0.6}Fe_{0.4}O₃ solid oxide fuel cell cathode by application of a thin interface cathode functional layer, *Mater. Lett.* 189 (2017) 252–255.
- [20] N. Hildenbrand, B.A. Boukamp, P. Nammensma, D.H. Blank, Improved cathode/electrolyte interface of SOFC, *Solid State Ionics* 192 (1) (2011) 12–15.
- [21] M. Benamira, M. Letilly, E. Quarez, O. Joubert, A.L.G. La Salle, Optimization of SOFC anode/electrolyte assembly based on Ba_{0.3}Ti_{0.7}O_{2.85}(BIT07)/Ni-BIT07 using an interfacial anodic layer, *J. Power Sources* 251 (2014) 66–74.
- [22] M. Benamira, A. Ringuede, M. Cassir, D. Horwat, J.F. Pierson, P. Lenormand, J. Fullenwarth, Comparison between ultrathin films of YSZ deposited at the solid oxide fuel cell cathode/electrolyte interface by atomic layer deposition, dip-coating or sputtering, *Open Fuel Energy Sci. J.* 2 (1) (2009) 87–99.
- [23] A.P. Kulkarni, S. Giddey, S.P.S. Badwal, Enhancing oxygen reduction reactions in solid oxide fuel cells with ultrathin nanofilm electrode electrolyte interfacial layers, *J. Phys. Chem. C* 120 (29) (2016) 15675–15683.
- [24] P. Briois, F. Perry, A. Billard, Structural and electrical characterisation of lanthanum nickelate reactively sputter-deposited thin films, *Thin Solid Films* 516 (2008) 3282–3286.
- [25] M.P. Pechini, Patent 3,330,697, 11th July 1967.
- [26] M.L. Fontaine, C. Laberty-Robert, A. Barnabé, F. Ansart, P. Tailhades, Synthesis of La₂-xNiO_{4+δ} oxides by polymeric route: non-stoichiometry control, *Ceram. Int.* 30 (2004) 2087–2098.
- [27] C. Brahim, A. Ringuede, E. Gourba, M. Cassir, A. Billard, P. Briois, Electrical properties of thin bilayered YSZ/GDC SOFC electrolyte elaborated by sputtering, *J. Power Sources* 156 (2006) 45–49.
- [28] B.A. Boukamp, A nonlinear least squares fit procedure for analysis of impedance data of electrochemical systems, *Solid State Ionics* 20 (1986) 31–44.
- [29] J. Wu, S.S. Pramana, S.J. Skinner, J.A. Kilner, A.P. Horsfield, Why Ni is absent from the surface of La₂NiO_{4+δ}? *J. Mater. Chem.* 3 (47) (2015) 23760–23767.
- [30] A.M. Hernández, L. Mogni, A. Caneiro, La₂NiO_{4+δ} as cathode for SOFC: reactivity study with YSZ and CGO electrolytes, *International Journal of Hydrogen Energy* 35 (11) (2010) 6031–6036.
- [31] N. Gauquelin, T.E. Weirich, M. Ceretti, W. Paulus, M. Schroeder, Long-term structural surface modifications of mixed conducting La₂NiO_{4+δ} at high temperatures, *Monatsh. Chem.* 140 (2009) 1095–1102.
- [32] R.K. Sharma, M. Burriel, L. Dessemond, J.M. Bassat, E. Djurado, La_n+1Ni_nO_{3n+1} (n = 2 and 3) phases and composites for solid oxide fuel cell cathodes: facile synthesis and electrochemical properties, *J. Power Sources* 325 (2016) 337–345.
- [33] Z. Lou, J. Peng, N. Dai, J. Qiao, Y. Yan, Z. Wang, K. Sun, High performance La₃Ni₂O₇ cathode prepared by a facile sol gel method for intermediate temperature solid oxide fuel cells, *Electrochem. Commun.* 22 (2012) 97–100.
- [34] Z. Zhang, M. Greenblatt, J.B. Goodenough, Synthesis, structure, and properties of the layered perovskite La₃Ni₂O_{7-δ}, *J. Solid State Chem.* 108 (2) (1994) 402–409.
- [35] F. Mauvy, C. Lalanne, J.-M. Bassat, J.-C. Grenier, H. Zhao, P. Dordor, Ph Stevens, Oxygen reduction on porous Ln₂NiO_{4+δ} electrodes, *J. Eur. Ceram. Soc.* 25 (2005) 2669–2672.
- [36] M.J. Escudero, A. Aguadero, J.A. Alonso, L. Daza, A kinetic study of oxygen reduction reaction on La₂NiO₄ cathodes by means of impedance spectroscopy, *J. Electroanal. Chem.* 611 (2007) 107–116.
- [37] E.J. Crumlin, E. Mutoro, S.J. Ahn, G.J. la O', D.N. Leonard, A. Borisevich, et al., Oxygen reduction kinetics enhancement on a heterostructured oxide surface for solid oxide fuel cells, *J. Phys. Chem. Lett.* 1 (21) (2010) 3149–3155.
- [38] R. Sayers, M. Rieu, P. Lenormand, F. Ansart, J.A. Kilner, S.J. Skinner, Development of lanthanum nickelate as a cathode for use in intermediate temperature solid oxide fuel cells, *Solid State Ionics* 192 (2011) 531–534.
- [39] H. Zhao, F. Mauvy, C. Lalanne, J.M. Bassat, S. Fourcade, J.C. Grenier, New cathode materials for ITSOFC: phase stability, oxygen exchange and cathode properties of La₂-xNiO_{4+δ}, *Solid State Ionics* 179 (35–36) (2008) 2000–2005.